Developmental Biology 395 (2014) 342–354

Contents lists available at ScienceDirect

Developmental Biology

journal homepage: www.elsevier.com/locate/developmentalbiology

Primary cilia function regulates the length of the embryonic trunk axis and urogenital field in mice

Elanor N Wainwright, Terje Svingen, Ee Ting Ng, Carol Wicking, Peter Koopman *

Institute for Molecular Bioscience, The University of Queensland, Brisbane QLD 4072, Australia

ARTICLE INFO

Article history:
Received 1 May 2014
Received in revised form
20 August 2014
Accepted 27 August 2014
Available online 16 September 2014

Keywords:
Gonad
Testis
Ovary
Organogenesis
Embryo patterning
Primary cilia

ABSTRACT

The issues of whether and how some organs coordinate their size and shape with the blueprint of the embryo axis, while others appear to regulate their morphogenesis autonomously, remain poorly understood. Mutations in *Ift144*, encoding a component of the trafficking machinery of primary cilia assembly, result in a range of embryo patterning defects, affecting the limbs, skeleton and neural system. Here, we show that embryos of the mouse mutant *Ift144*^{twt} develop gonads that are larger than wild-type. Investigation of the early patterning of the urogenital ridge revealed that the anterior–posterior domain of the gonad/mesonephros was extended at 10.5 dpc, with no change in the length of the metanephros. In XY embryos, this extension resulted in an increase in testis cord number. Moreover, we observed a concomitant extension of the trunk axis in both sexes, with no change in the length of the tail domain or somite number. Our findings support a model in which: (1) primary cilia regulate embryonic trunk elongation; (2) the length of the trunk axis determines the size of the urogenital ridges; and (3) the gonad domain is partitioned into a number of testis cords that depends on the available space, rather than being divided a predetermined number of times to generate a specific number of cords.

Introduction

Embryonic development is orchestrated through an orderly and interconnected progression of events in a precise temporal and spatial sequence. Disruptions in the meshwork of events affecting one tissue can alter the patterning of neighbouring organ systems and have "knock-on" effects in the differentiation and function of their neighbours. In the trunk of the embryo, it is unclear which organs align their development and morphology with the embryo axis rather than having more autonomous regulation of their size and shape.

In mice, the urogenital system is derived from the linear and sequential differentiation of three kidney primordia arising from the intermediate mesoderm. At 8.0 dpc, a portion of the intermediate mesoderm on both sides of the midline undergoes mesenchymal-to-epithelial transition to form the Wolffian ducts, which subsequently extend in a posterior direction until they terminate in the cloaca (Bouchard et al., 2002; Grote et al., 2006). The first primordial kidney—the pronephros—degenerates almost as soon as it forms (Bouchard et al., 2002). Subsequently, the second primordial kidney—the mesonephros—differentiates and will go on to form the reproductive tract. The gonad forms on the ventromedial surface of the mesonephros at 10.5 dpc. At the level of the hindlimb, the remaining intermediate mesoderm condenses and interacts with the Wolffian duct to induce the outgrowth of the final definitive kidney, the metanephros (Saxen and Sariola, 1987).

The gonad develops on the surface of the mesonephros between 9.5 and 10.5 dpc, when coelomic epithelial cells proliferate and undergo epithelial-to-mesenchymal transition to form gonadal somatic cells (Karl and Capel, 1998). Primordial germ cells (PGCs) are specified at the proximal end of the epiblast from where they move to the extra-embryonic mesoderm at the base of the allantois at an earlier stage, around 6.5 dpc (Lawson and Hage, 1994; McLaren and Lawson, 2005; Ohinata et al., 2005). From the extraembryonic mesoderm, PGCs migrate to the hindgut endoderm and subsequently traverse the hindgut mesentery between 9.5 and 10.5 dpc to reach their final destination, the genital ridges (Ginsburg et al., 1990). It has been hypothesised that the long and narrow gonadal structure has evolved to act as a "net" to receive germ cells dispersed in the hindgut (Harikae et al., 2013), but how the size and shape of the gonad domain is regulated remains poorly understood.

The primary cilium is an immotile cellular organelle that protrudes from most non-dividing vertebrate cells (Goetz and Anderson, 2010). In humans and mice, mutations leading to either disruption of primary cilium biogenesis or function can have severe developmental consequences resulting in disorders and diseases collectively referred

* Corresponding author. Fax: +61 7 3346 2101.
E-mail address: p.koopman@imb.uq.edu.au (P. Koopman).

http://dx.doi.org/10.1016/j.ydbio.2014.08.037
0012-1606/

to as ciliopathies. This large, heterogeneous group of disorders includes polycystic kidney disease and retinal pigmentosa, as well as more complex syndromes with variable phenotypes such as Bardet-Biedl, Jeune, short rib polydactyly and Sensenbrenner syndromes. Frequent phenotypes associated with primary cilium defects include skeletal abnormalities, renal cysts, retinal degeneration and neurological defects (Goetz and Anderson, 2010).

In addition to having a mechanosensory role, primary cilia act as a signalling hub and are functionally linked to the Hh, WNT, NOTCH, PDGFRα, FGF and HIPPO pathways (Corbit et al., 2005; Ezratty et al., 2011; Habbig et al., 2012; Neugebauer et al., 2009; Schneider et al., 2005). Proteins are dynamically trafficked up and down the microtubule-based ciliary axoneme using a specialised motor-driven trafficking process known as intraflagellar transport (IFT) (Pazour et al., 2000). Generally, a group of anterograde trafficking proteins (IFT-B) move cargo to the tip of the cilium using a kinesin motor protein complex, whereas retrograde trafficking proteins (IFT-A) move cargo from the tip to the base via a dynein motor protein complex (Ou et al., 2005).

The IFT-A gene *Ift144* (or *Wdr19*) has been linked to both Jeune asphyxiating thoracic dystrophy syndrome and Sensenbrenner or cranio-ectodermal dysplasia syndrome (Bredrup et al., 2011; Fehrenbach et al., 2014). Previous analysis of a mouse model with a hypomorphic missense mutation of *Ift144* ("twinkle-toes", or *Ift144*^{twt}), revealed a number of characteristics of the cognate human diseases, including polydactyly, short rib cage, limb truncation, neural patterning and cleft lip/palate (Ashe et al., 2012; Liem et al., 2012). Rib defects in *Ift144*^{twt} mouse mutants were shown to result from early disrupted somitic patterning in the inter-limb region. In addition, *Ift144*^{twt} embryos have fewer primary cilia, but only very subtle changes to the structure of those primary cilia that do form. Furthermore, embryonic fibroblasts derived from *Ift144*^{twt} embryos display an attenuated response to upstream activation of Hh signalling, whereas analysis *in vivo* revealed a ligand-independent expansion of Hh signalling in some contexts (Ashe et al., 2012; Liem et al., 2012).

In the present study we show that, in addition to the defects previously described, *Ift144*^{twt} mutants display hyperplastic gonads in both XX and XY embryos. Underlying this significant increase in gonad size, *Ift144*^{twt} mice had an early anterior expansion of the gonad domain along the anterior-to-posterior axis, concomitant with an extension in the length of the embryo trunk. These findings help to define the underlying mechanisms of gonad morphogenesis and dependency of organ patterning on the embryonic axis.

Materials and methods

Mice

Ift144^{twt} mice have been described previously and were analysed on a FVB/NJ background (Ashe et al., 2012) and were compared to wild-type littermates. Oct4-GFP strain has also been reported previously (Szabo et al., 2002). For detection of primary cilia in embryonic gonad development, wild-type embryos were collected from timed matings of outbred CD1 strain mice. Mice were staged with noon of the day on which the mating plug was observed designated 0.5 days post-coitum (dpc) and 8–10 tail somite (ts) correlating to 10.5 dpcdpc and 17–18 ts correlating to 11.5 dpc. Sx PCR was used to determine the sex of the embryos (McFarlane et al., 2013). Protocols and use of animals were approved by the Animal Ethics Committee of the University of Queensland, which is registered as an institution that uses animals for scientific purposes under the Queensland Animal Care and Protection Act (2001).

Immunofluorescence

The following primary antibodies against endogenous mouse antigens were used in immunofluorescence; rabbit anti-MVH (code 13840; Abcam) used at 1:400 dilution; mouse anti-E-cadherin (code 610182, Becton Dickinson) used at 1:200 dilution; mouse anti-SOX9 (code H00006662-M01; Abnova) used at 1:200 dilution; rabbit anti-FOXL2 (Polanco JC 2010) used at 1:600 dilution; mouse anti-ARL13B (code 75-287; Antibodies Incorporated) used at 1:200 dilution; mouse anti-OCT4 (code sc-5279; Santa Cruz) used at 1:100 dilution; goat anti-AMH (code SC-5279; Santa Cruz); chicken anti-GFP (code 13970; Abcam) used at 1:400 dilution; goat anti-GATA4 (code sc-1237; Santa Cruz) used at 1:100 dilution, rabbit anti-PAX2 (code 71–6000; Invitrogen) used at 1:200 dilution, Mouse anti-MVH (code ab27591; Abcam) used at 1:600 dilution and rabbit anti-STRA8 (code ab49405; Abcam) used at 1:200 dilution. The secondary antibodies used were donkey anti-goat Alexa 488 (code A11055; Invitrogen) at 1:200 dilution; goat anti-rabbit Alexa 594 (code A11034; Invitrogen) at 1:200 dilution; donkey anti-rabbit Alexa 568 (code A10042; Invitrogen) at 1:200 dilution; and 40,6-diamidino-2-phenylindole (DAPI; 2 ng/μl in PBS; Molecular Probes) at 1:1000 dilution to visualise nuclear DNA in immunofluorescence.

For section immunofluorescence, 7 μm paraffin sections were processed as described previously (Polanco JC 2010). Slides were imaged using a confocal microscope (LSM 510 Meta; Zeiss). For whole-mount immunofluorescence, dissected gonads/mesonephroi were fixed in 4% paraformaldehyde (PFA) in PBTX (PBS containing 0.1% Triton X-100) overnight at 4 °C. Samples were washed in phosphate buffered Saline (PBS) and stored in 100% methanol (MeOH) at −20 °C until required. Samples were rehydrated through at MeOH series and then blocked for 4 h at room temperature in 10% heat inactivate horse serum (HS)/PBTX. Primary antibody was incubated overnight at 4 °C and then washed at least three times in PBTX for a minimum of 24 h. Subsequently, the secondary antibody was incubated overnight at 4 °C diluted in 10% HS/PBTX and then washed three times in PBTX for a minimum of 24 h. Samples were dehydrated into 100% methanol before being cleared by 1:2 benzyl alcohol/benzyl benzoate (BABB). Samples were mounted in a glass bottom dish (code P35G-1.5-14-C, MatTek corporation) and imaged using an inverted LSM 510 Meta (Zeiss) confocal microscope.

Image capture, analysis and processing

For wholemount immunofluorescence, serial non-overlapping Z-slice optical sections were captured for the depth of the sample. For 13.5 dpc XY gonads, samples were imaged on 10× objective at 7.1 μm intervals. For 10.5 dpc urogenital ridges, samples were imaged on a 10x objective with a 0.8× optical zoom, tiled over two different fields of view at 7.1 μm intervals. Optical sections were processed in Imaris software (Bitplane) to produce maximum intensity projections and testis cord 3D models with the rendering tool: surfaces. Whole-mount pictures of embryos and dissected tissue were captured on Olympus SZX-12 stereomicroscope.

Image quantification

Number of somites and embryo lengths were quantified on *Ift144*^{twt} and wild-type littermate control embryos previously stained by *in situ* hybridisation to reveal somite markers (Ashe et al., 2012). For measuring embryo dimensions and urogenital ridge lengths, samples were imaged in the same orientation at the same magnification and then the length of each sample was measured using drawing tools in ImageJ software. Testis cords were counted from the coelomic view of rendered testis cord models. For quantification of number of cells in the testis, the one sagittal section through the centre of the testis (the largest plane)

was used for quantification per sample (2582, 2555 and 2676 total number of cells counted per *Ift144*^{twt} testis, and 1666, 1718 and 1753 total cells counted per wild-type testis) using the manual ImageJ cell counter tool. $n=3$. Germ cells were marked by E-cadherin, Sertoli cells by strong expression of GATA4, Leydig cells by HSD3β and interstitial/peritubular myoid cells by weak expression of GATA4.

Haematoxylin and eosin staining

Paraffin sections (7 μm) were de-waxed in xylene, rehydrated through an ethanol series. stained with freshly filtered haematoxylin, washed, and counterstained in eosin solution. Finally, slides were dehydrated, cleared in xylene, mounted in Entellan mounting medium (Millipore) and imaged with a BX-51 microscope (Olympus).

Quantitative RT-PCR

Quantitative RT-PCR (qRT-PCR) using SYBR green (Invitrogen) was performed as described previously (Svingen et al., 2009), using gonad samples from which the mesonephroi had been removed ($n=6$). Samples were normalised to the endogenous housekeeping gene *Sdha* (Svingen et al., 2009). Subsequently, gene expression levels were analysed using unpaired two-tailed Student *T*-tests (PRISM version 5.0 software; GraphPad). The SYBR green primers used in this study are described in Supplemental Table S1.

Results

Primary cilia are localised to the gonad interstitium

To address the possible signalling interactions mediated by primary cilia in the foetal gonad, we first investigated whether and which embryonic gonadal cells have a primary cilium in both sexes at 10.5 dpc, 11.5 dpc and 13.5 dpc. The presence of cilia was determined by immunoreactivity of ARL13B, a required functional component of the primary cilium (Duldulao et al., 2009). In both sexes at 10.5 and 11.5 dpc, a primary cilium was commonly detected in somatic cells marked by SF-1 and in some germ cells (Fig. 1A, B, D and E). In addition, a primary cilium was detected in some Sertoli cells at 11.5 dpc (Fig. 1C). In the testis at 13.5 dpc, primary cilia were detected in the interstitium and rarely in testis cords. Specifically, a primary cilium was detected in HSD3β-positive differentiated Leydig cells, HSD3β-negative cells, and in peritubular myoid cells (Fig. 1F and G). These observations were consistent with the interstitial cell population undergoing active hedgehog signalling at this time point (Yao et al., 2002). Interestingly, a primary cilium was rarely detected in Sertoli cells, marked by AMH expression, or in germ cells, marked by MVH expression (Fig. 1G and H).

The foetal ovary can be regionally compartmentalised by marker gene expression, with a population of somatic cells at or near the coelomic epithelium being molecularly distinct from those cells a few layers adjacent to the mesonephros (Chen et al., 2012). We detected primary cilia frequently in ovarian cells at 13.5 dpc at and towards the coelomic epithelium (Fig. 1I), but also in the few cell layers adjacent to the mesonephros (Fig. 1J). A few of the FOXL2-positive somatic cells destined to become medullary granulosa cells, also had a primary cilium (Fig. 1J). In contrast to testicular germ cells, a primary cilium was detected in some ovarian germ cells (Fig. 1K). In summary, most cell types in the ovary were found to produce a primary cilium, albeit not all, and are therefore likely to have some capacity for cilia-mediated signalling.

Increased size of Ift144^{twt} *gonads*

To investigate potential reproductive complications of Jeune and Sensenbrenner syndromes, we examined the urogenital system of *Ift144*^{twt} mice just prior to birth, at 17.5 dpc. While there was no overall size difference between *Ift144*^{twt} and wild-type embryos (Fig. 2A), *Ift144*^{twt} testes and ovaries were strikingly and consistently larger (Fig. 2B). The other organs that together comprise the urogenital system were of similar size to wild-type. In addition, *Ift144*^{twt} ovaries were mis-localised to a more anterior position on the ventral face of the kidney, relative to wild-type (Supplemental Fig. S1A). In most cases, the formation of the male and female reproductive tracts was normal, with one of eight XY embryos displaying a unilateral dilated and uncoiled epididymis (Supplemental Fig. S1B).

The histology of the ovaries and testes at 17.5 dpc was assessed by haematoxylin and eosin (H&E) staining (Fig. 2C). The *Ift144*^{twt} ovaries showed a similar cell density to wild-type, suggesting that there were more cells overall. On the other hand, the interstitial stroma of *Ift144*^{twt} testes was less closely packed compared to wild-type, suggesting either a reduction in the number of cells and/or that the cells were less condensed. Immunofluorescence for HSD3β expression, a marker of differentiated Leydig cells, showed that both Leydig cells and HSD3β-negative interstitial stromal cells were present, which suggests that there was no defect in Leydig cell differentiation (Fig. 2D).

Having established that *Ift144*^{twt} gonads were abnormally large at 17.5 dpc, we sought to determine the developmental stage at which the increase in size occurs. At 13.5 dpc, after sex differentiation of the gonads, *Ift144*^{twt} testes and ovaries were clearly longer compared to wild-type gonads (Fig. 3A). The gonad domain was extended anteriorly beyond the level of the kidney, suggesting that an anterior expansion of the mesonephric-gonad domain may have occurred (Supplemental Fig. S2A,B). Examination of the urogenital ridge revealed that *Ift144*^{twt} adrenals were also bigger (Supplemental Fig. S2C), while *Ift144*^{twt} kidneys were the same size as wild-type (Fig. 3A). This is consistent with an expansion of the mesonephric but not the metanephric domain.

XY Ift144^{twt} *gonads have additional testis cords at 13.5 dpc*

Testis cords are required to create a shielded, avascular and immune-privileged environment for developing spermatozoa. In the XY gonad, testis cord morphogenesis proceeds with Sertoli cells clustering around groups of germ cells, followed by endothelial cells from the mesonephros migrating into the gonad to partition Sertoli and germ cell clusters into cord domains (Combes et al., 2009b; Cool et al., 2008; Coveney et al., 2008). Since the gonad domain is longer in *Ift144*^{twt} embryos, we investigated the consequences for the architecture of the testis cords. At 13.5 dpc, testis cords have just formed and are arranged as a stack of toroidal loops along the gonad axis. Three-dimensional rendering of testis cords based on Sertoli cell-specific AMH expression revealed a similar shape and size between mutant and wild-type gonads (Fig. 3B). However, *Ift144*^{twt} testes contained significantly more cords compared to wild-type, with an average increase of 4.8 cords (Fig. 3C). These data support a model in which the XY gonad domain is partitioned into testis cords along the available space, rather than divided a predetermined number of times to generate a specific number of cords.

Gonadal sex differentiation proceeds normally in Ift144^{twt} *gonads*

To investigate any changes in gonad differentiation, we examined the expression of several important genes that mark the various testicular and ovarian cell lineages at 13.5 dpc by quantitative RT-PCR. In the testis, there was no significant change in the expression of the Sertoli cell marker *Sox9*, the germ cell marker

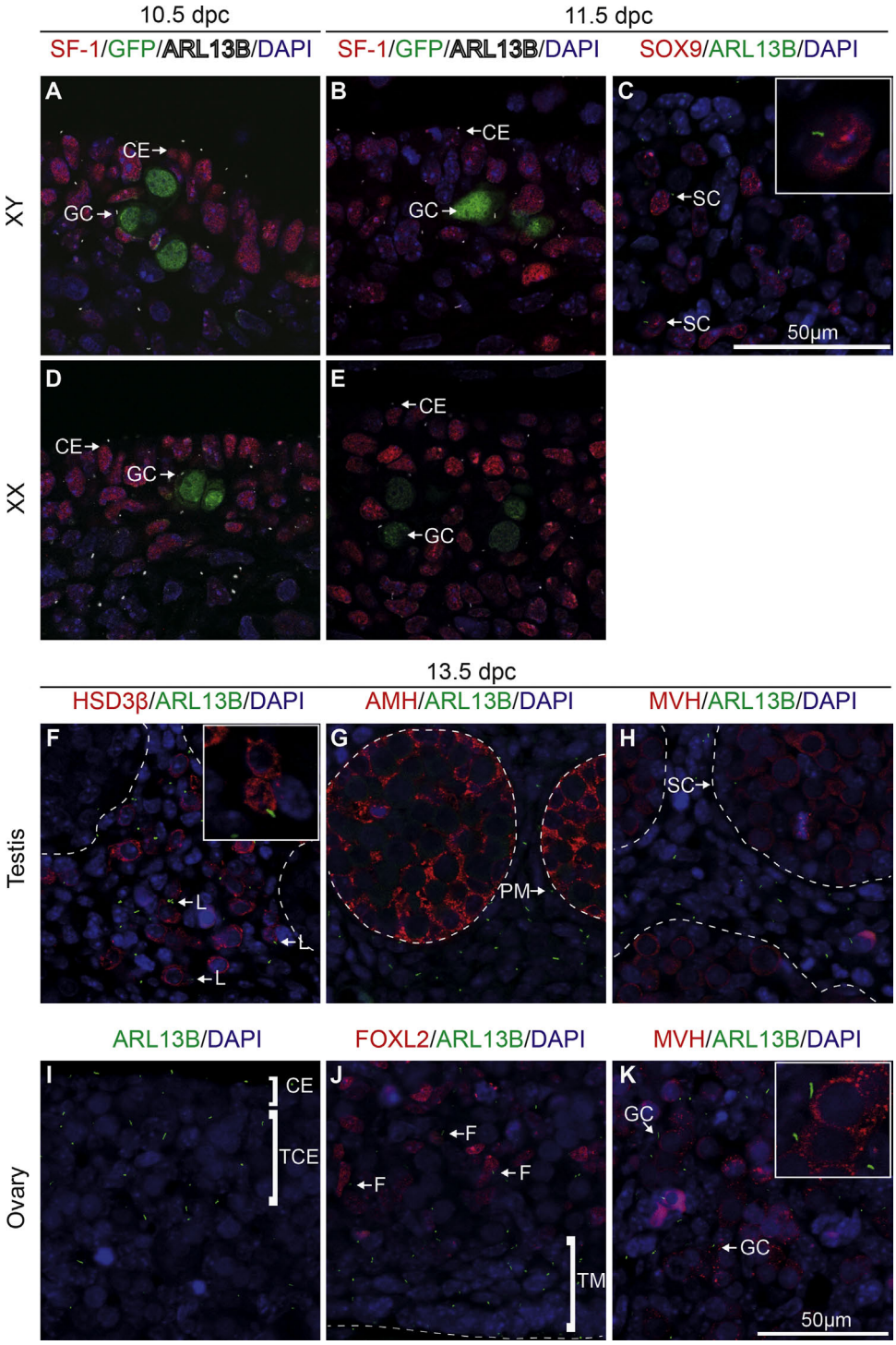

Fig. 1. Primary cilia are detected in the testis and ovary at 10.5 dpc, 11.5 dpc and 13.5 dpc. (A, B, D, F) Immunofluorescence on paraffin sections of 10.5 and 11.5 dpc OCT4-GFP wild-type embryos for ARL13B (white), detected primary cilia, GFP (green), detected germ cells, SF-1 (red) detected gonad somatic cells (red). (E) Section immunofluorescence at 11.5 dpc for SOX9 (red), detected Sertoli cells and ARL13B (green), detected primary cilia. Immunofluorescence on paraffin sections of 13.5 dpc wild-type embryos for ARL13B (green), detected primary cilia and: (F) HSD3β (red), detected Leydig cells in the testis; (G) AMH (red) detected Sertoli cells in the XY gonad; (H) MVH (red) detected germ cells in the testis; (J) FOXL2 (red) detected somatic cells in the ovary and; (K) MVH (red) detected germ cells in the ovary. DAPI (blue) marking cell nuclei. Dotted line in (J) indicates gonad-mesonephric boundary. Arrows indicate cell type with a primary cilium. Abbreviations: L, Leydig cell; PM, pertitubular myloid cell; SC, Sertoli cell; CE, coelomic epithelium; TCE, Towards the coelomic epithelium; F, FOXL2 positive somatic cells; TM, Towards the mesonephros; and GC, germ cells. Scale bar, 50 μm.

Mvh, the somatic cell marker *Nr5a1*, or the Leydig cell marker *Scc*. Quantification of the number of germ cells, Sertoli cells, Leydig cells and interstitial/peritubular myoid cells in the largest cross-sectional area through the testis did not identify any significant difference between the proportion of each cell lineage in *Ift144*^{twt} testes, compared to wild-type (Supplemental Fig. S3). In addition, there was no ectopic up-regulation of the ovarian somatic cell markers *Foxl2* and *Wnt4* (Fig. 4). In the ovary, examination of cell-specific markers revealed that the expression of *Wnt4* was significantly reduced, but no other significant changes had occurred.

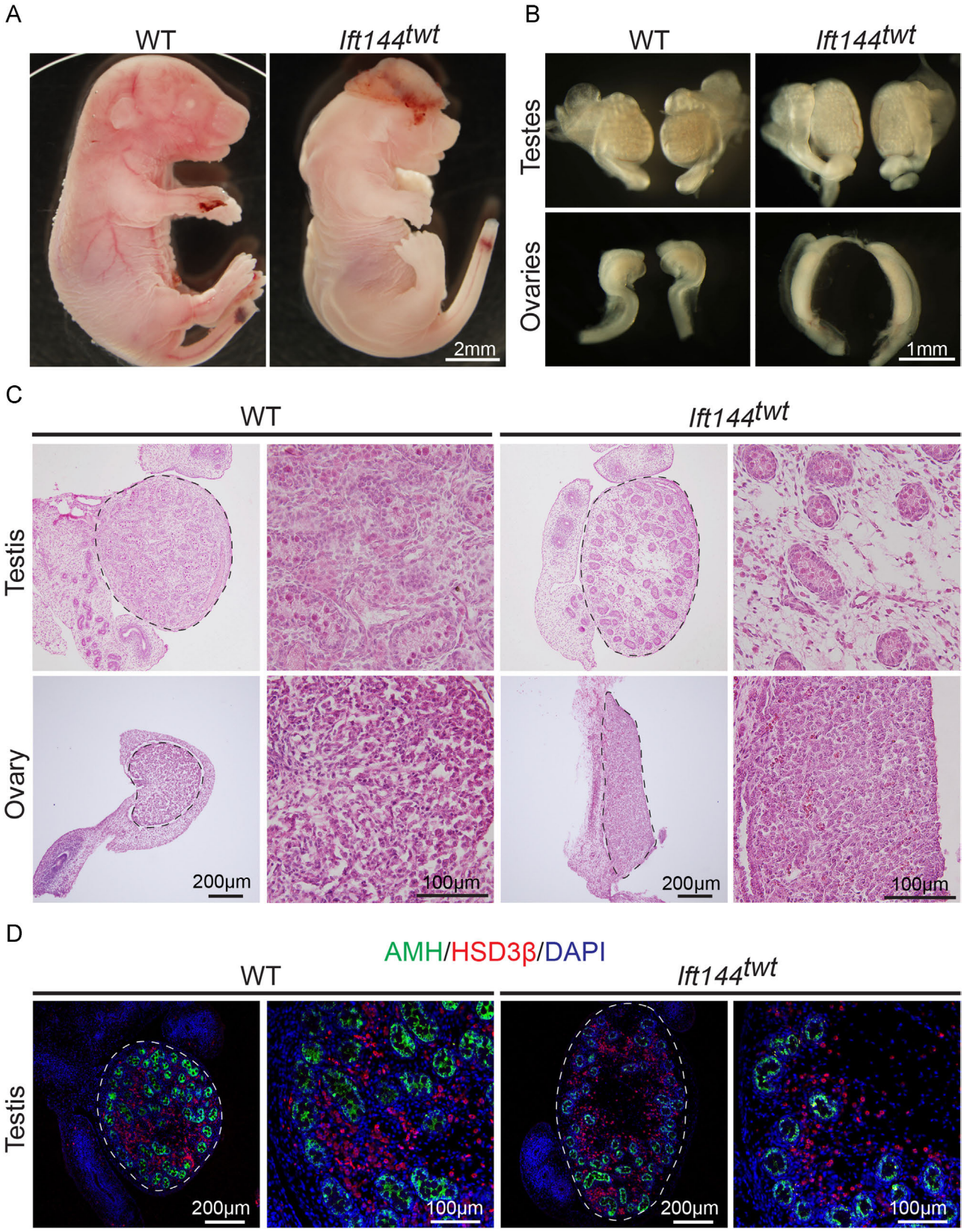

Fig. 2. Enlarged gonads in *Ift144*^{twt} mice at 17.5 dpc. (A) *Ift144*^{twt} embryos are a similar size to wild-type (WT) embryos at 17.5 dpc. Scale bar, 2 mm. (B) Brightfield images of dissected testes and ovaries indicated that *Ift144*^{twt} mice have enlarged gonads. Scale bar, 1 mm. $n=5$. (C) Haematoxylin and eosin staining of gonad sections showed that the testicular interstitium is less compact. Scale bar, 200 μm. $n=4$. (D) Section immunofluorescence for HSD3β (red), marking Leydig cells, and AMH (green), marking Sertoli cells, indicated that Leydig and non-Leydig cells are present in the interstitium. Cell nuclei are stained with DAPI (blue). $n=4$. Scale bar, 200 μm.

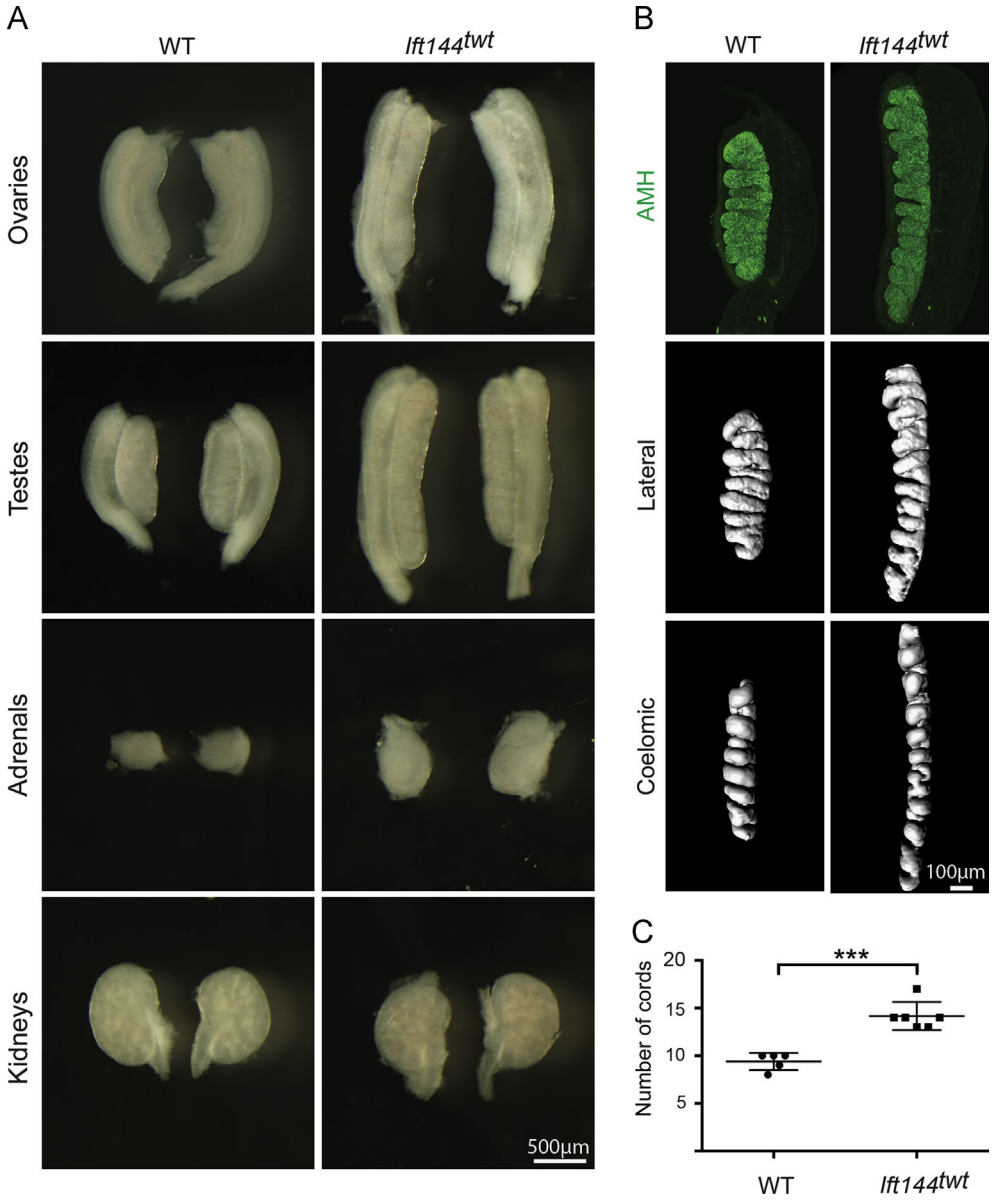

Fig. 3. Increased number of cords in *Ift144*^{twt} testes. (A) Brightfield images of dissected urogenital complex at 13.5 dpc, showing that *Ift144*^{twt} ovaries and testes are longer than wild-type (WT). Scale bar, 500 μm. $n=3$ (B) Wholemount immunofluorescence for AMH (green) was used to demarcate the testis cords and create a three dimensional testis cord rendering (grey). Scale bar, 100 μm. (C) Quantification of testis cords identified a significant increase in the number in XY *Ift144*^{twt} gonads. Unpaired two-tailed Student's *T*-test was used to assess statistical significance. $n=3$, left and right gonads imaged. $^{***}p<0.001$.

Interestingly, all ovaries examined showed an increase in expression of *Scc*, albeit to a highly variable extent and not statistically significant.

The signalling pathway most strongly linked to primary cilia is the Sonic hedgehog (*Shh*) pathway. Although *Shh* is absent from the foetal gonads, Desert hedgehog (*Dhh*) and its shared downstream effector genes *Gli1* and *Gli2* are all essential for normal testis differentiation. Genetic loss of *Dhh* results in a reduction in the number of Leydig cells in XY gonads, whereas constitutive Hh signalling in XX gonads result in ectopic Leydig cell development, demonstrating that Hh signalling is both necessary and sufficient for Leydig cell differentiation (Barsoum et al., 2009; Yao et al., 2002). Therefore, we examined the expression of *Dhh* signal transduction components in *Ift144*^{twt} testes and ovaries at 13.5 dpc. In testes and ovaries, hedgehog pathway components *Dhh*, *Ptch1*, *Ptch2*, *Gli1*, *Gli2* and *Hhip*, were expressed at normal levels compared to wild-type (Fig. 4).

Examination of *Ift144*^{twt} embryos by section immunofluorescence revealed normal sex differentiation of *Ift144*^{twt} gonads compared to wild-type. Both germ cells and SOX9 positive cells in the testis, and germ cells and FOXL2 positive cells in the ovary, spanned the length of the gonad to the anterior and posterior poles (Fig. 5A and B). Furthermore, Leydig cell differentiation occurred normally in *Ift144*^{twt} testes, as assessed by *Scc* staining, and no ectopic *Scc* expression was detected in *Ift144*^{twt} ovaries (Fig. 5C).

Previously, XY *Map3k1*-null mice were found to have ~16% longer gonads at 13.5 dpc and to develop ectopic STRA8-positive germ cells in the posterior gonadal pole (Warr et al., 2011). It was postulated that the increase in gonad length may have hindered the centre-to-pole expansion of the testis-determining gene expression pathway, resulting in germ cells ectopically entering meiosis at the posterior pole (Warr et al., 2011). However, we found no STRA8 expression in XY *Ift144*^{twt} gonads, suggesting that an expansion of the XY gonad domain length does not inhibit the male gene expression pathway (Supplemental Fig. S4). Therefore, despite the increase in gonad length, the molecular sex differentiation and patterning of *Ift144*^{twt} gonads appeared normal.

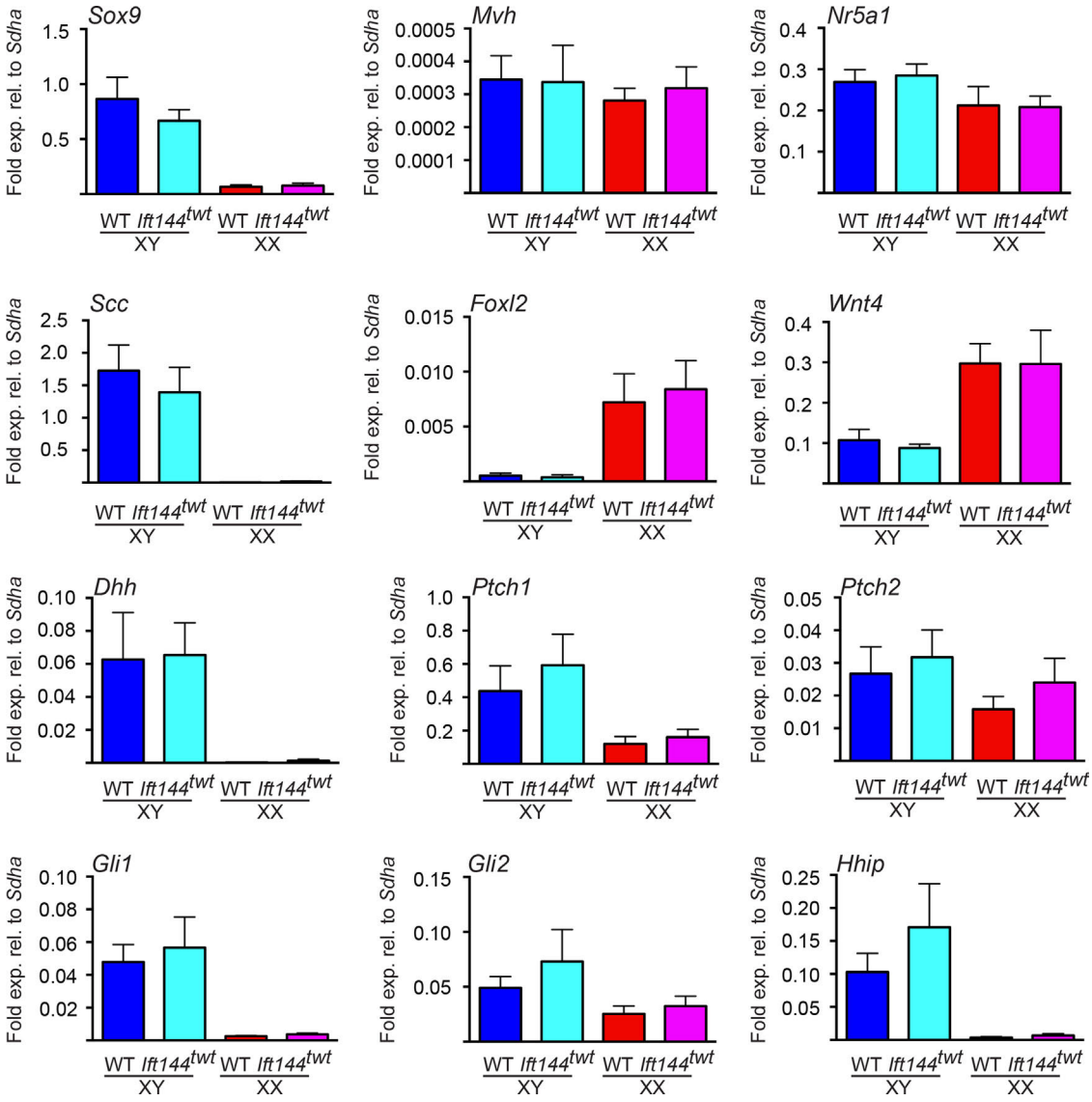

Fig. 4. Gene expression analysis in *Ift144*^{twt} gonads. Quantitative RT-PCR did not detect any significant changes in the expression of the Sertoli cell marker, *Sox9*, germ cell marker, *Mvh*, somatic cell marker, *Nr5a1*, Leydig cell marker, *Scc*, ovarian somatic cell marker, *Foxl2*, relative to wild-type (WT). The ovarian somatic cell marker *Wnt4* was significantly reduced in the *Ift144*^{twt} ovary compared to WT. Quantitative RT-PCR did not detect any significant changes in the expression of the hedgehog pathway component genes *Dhh*, *Ptch1*, *Ptch2*, *Gli1*, *Gli2*, *Hhip*, although variable up-regulation of *Ptch1*, *Gli1*, *Gli2* and *Hhip* was detected in *Ift144*^{twt} ovaries. Error bars represent SEM, $n=6$. Unpaired two-tailed Student's *T*-test was used to assess statistical significance, $^{*}p<0.05$.

The anterior–posterior gonad domain is expanded by 10.5 dpc

To determine the cause of the dramatic increase in gonadal length in *Ift144*^{twt} embryos, we examined urogenital ridges at 10.5 dpc, the earliest time point in gonad development. Whole mount immunofluorescence for PAX2, a marker of the Wolffian duct and metanephric mesenchyme, and GATA4, a marker of the coelomic epithelium/somatic cells of the gonad, revealed that the *Ift144*^{twt} urogenital ridges were longer than those in wild-type embryos (Fig. 6A). Quantification confirmed that the gonad/mesonephric domain was expanded in *Ift144*^{twt} mutants by on average 30% (Fig. 6B). Interestingly, the length of the metanephros, the region of definitive kidney formation, was unchanged, consistent with our earlier observations that kidney size was normal in *Ift144*^{twt} mutant mice at later developmental stages (Fig. 6C).

Quantification of the number of mesonephric tubules and distribution of mesonephric tubule domain did not detect any significant difference between *Ift144*^{twt} mutant and wild-type embryos (Fig. 6D and E), suggesting that there was no change in the amount of intermediate mesoderm specified (Kume et al., 2000; Mattiske et al., 2006). In addition, germ cells marked by OCT4 had a similar distribution in the gonad domain of *Ift144*^{twt} mutant embryos compared to wild-type (Fig. 6F), supporting our earlier observations that gonad poles of *Ift144*^{twt} mutant embryos were correctly patterned at 13.5 dpc.

To determine if changes to gonad-intrinsic hedgehog signalling could be responsible for the expanded gonad/mesonephric domain phenotype, the expression of the direct hedgehog target genes *Gli1* and *Ptch1* was assessed at 10.5 dpc. In both *Ift144*^{twt} mutant and wild-type urogenital ridges, expression of *Gli1* and *Ptch1* were detected as similar levels in the mesonephros and were undetectable in the gonad (Supplemental Fig. S5). Therefore, perturbation to hedgehog signalling in the gonad primordium is unlikely to cause gonad/mesonephric expansion.

The embryo trunk region is expanded

Upon dissection of 10.5 dpc urogenital ridges, we noticed that despite a clear anterior expansion of the gonad domain, the urogenital

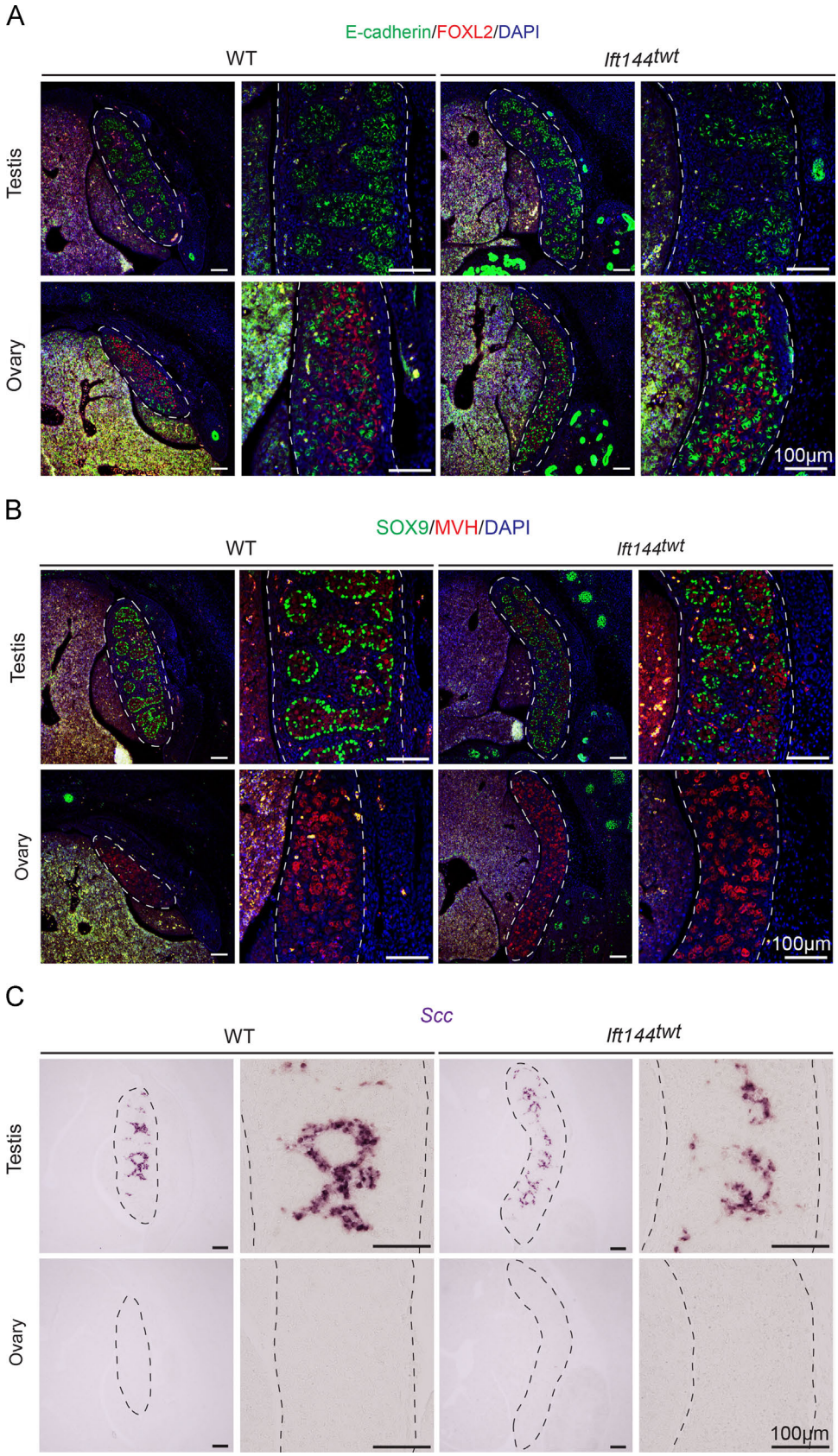

Fig. 5. Normal sex-specific development of the gonads in *Ift144*^{twt} embryos at 13.5 dpc. (A) Immunofluorescence on paraffin sections for E-cadherin (green), marking germ cells and FOXL2 (red), marking female somatic cells, indicates no changes in the distribution of germ cells and expression of FOXL2 in *Ift144*^{twt} ovaries and testes, compared to wild-type (WT). $n=3$. Scale bars, 100 μm. (B) Section immunofluorescence for SOX9 (green), marking Sertoli cells and MVH (red), marking germ cells, indicates no changes in the distribution of germ cells and expression of SOX9 in *Ift144*^{twt} ovaries and testes, compared to wild-type (WT). $n=3$. Scale bars, 100 μm. (C) Section *in situ* hybridisation for *Scc* (purple) did not detect any ectopic Leydig cells in *Ift144*^{twt} ovaries, compared to wild-type (WT). $n=4$ Scale bars, 100 μm. Gonad tissue is marked by a dotted line. Gonads were examined at 12.5, 13.5, 15.5 and 17.5 dpc.

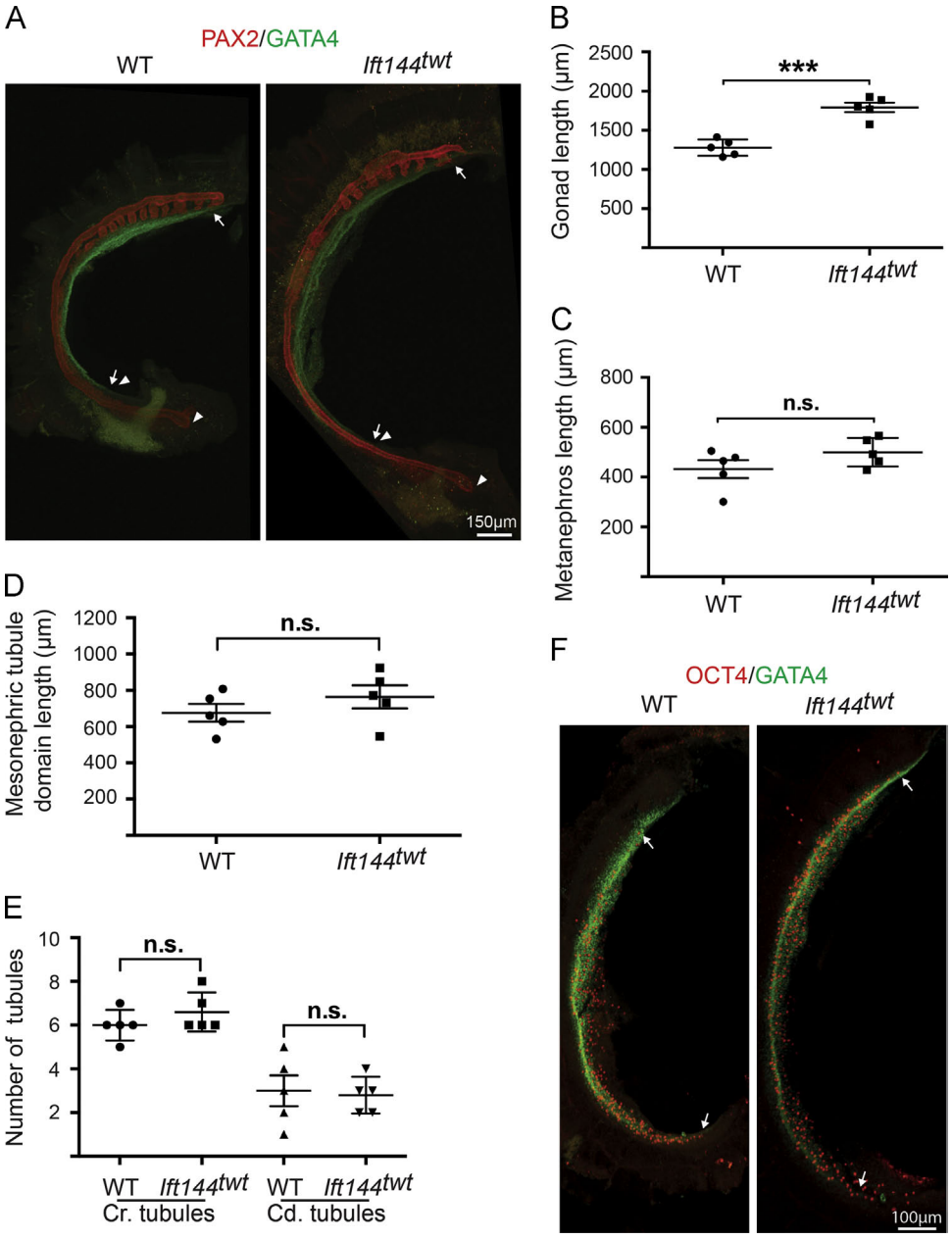

Fig. 6. The anterior–posterior axis of the gonad is expanded in *Ift144*^{twt} mice. (A) Confocal images of wholemount immunofluorescence for PAX2 (red), marking the Wolffian duct, mesonephric tubules and metanephric mesenchyme, and GATA4 (green), marking the gonad somatic cells and coelomic epithelium, indicates that the gonad is extended in *Ift144*^{twt} mice. Arrows show anterior and posterior boundaries of the gonad domain and arrowheads indicate anterior and posterior boundaries of the metanephros. Images were taken at the same magnification; scale bar, 150 μm. (B) Quantification at 10.5 dpc shows that the gonad length was expanded, whereas the length of the metanephros (C) was unchanged, compared to wild-type (WT). (D) Quantification of the length of the mesonephric tubule domain and (E) the number of cranial (Cr) and caudal (Cd) mesonephric tubules did not detect any significant difference between *Ift144*^{twt} mutant and wild-type urogenital ridges. Unpaired two-tailed Student's *T*-test was used to assess statistical significance. $^{***}p < 0.001$, n.s. not significant. $n=5$. (F) Confocal images of wholemount immunofluorescence for OCT4 (red), marking the germ cells, and GATA4 (green), marking the gonad somatic cells and coelomic epithelium, indicates that germ cells have a similar distribution in the gonad at 10.5 dpc between *Ift144*^{twt} mutant and wild-type embryos. $n=3$.

ridge did not appear to be localised any higher in the body cavity relative to the forelimb. Therefore, we examined whole embryo patterning to determine if any changes in embryo length had occurred. It was previously noted that *Ift144*^{twt} embryos have similar number of tail somites to wild-type littermates (Ashe et al., 2012). Furthermore, it was shown that the shape of the somites was perturbed specifically in the trunk region of the embryo (Ashe et al., 2012). We counted the number of somites in the trunk (base of forelimb to top of hind limb) and tail (base of hind limb to tail tip) regions of embryos highlighted by *in situ* hybridisation for the somite marker *MyoD* at 10.5 dpc and 11.5 dpc (Fig. 7A and data not shown). Supporting previous observations, the shape of the somites was perturbed particularly in the inter-limb region correlating to the T1–T13 vertebral elements, which is also the same region of the embryo containing the gonad domain (Fig. 7B). No significant changes had occurred in the number of somites in either the tail or trunk region of *Ift144*^{twt} embryos (Fig. 7C and D). However, the length of the trunk was significantly increased whereas the length of the tail was unchanged (Fig. 7E and F). Because the gonad domain normally spans the length of the trunk region, it is likely that the trunk expansion is the underlying cause of the increase in the gonad domain in *Ift144*^{twt} embryos.

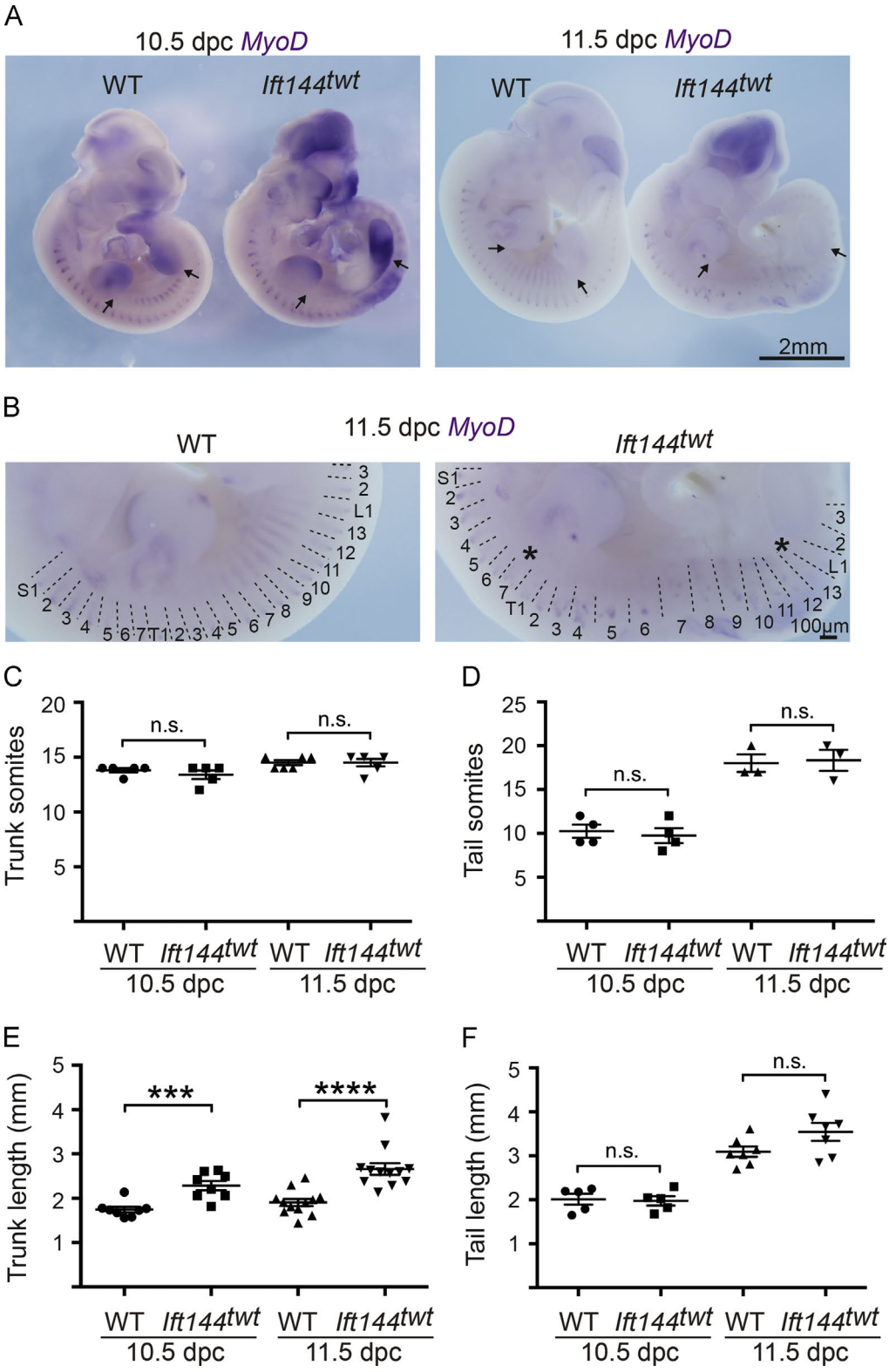

Fig. 7. Expansion of the embryo trunk domain in *Ift144*^{twt} embryos. (A) Wholemount *in situ* hybridisation for *MyoD* at 10.5 dpc and 11.5 dpc was used to demarcate the somites, showing that the embryo trunk was expanded. Scale bars, 2 mm. (B) Magnified regions of *MyoD* expression at 11.5 dpc show that the somites specifically between the fore- and hindlimb were disrupted. The region of disruption is indicated by asterisks. Scale bars, 100 μm. Quantification revealed no significant change in trunk (C) and tail (D) somite number, with a significant increase in the length of the trunk (E) but not the tail (F) region. Unpaired two-tailed Student's *T*-test was used to assess statistical significance $^{***}p < 0.001$, $^{****}p < 0.0001$, n.s. not significant. $n = 3–12$.

Discussion

The paradigm of gonad domain specification is poorly understood. Here, we have shown that mouse mutants with dysfunctional primary cilia display an early expansion of the anterior–posterior gonad axis associated with extension of the embryo trunk. As a consequence, the XY gonads were found to be partitioned into additional testis cords. Our data suggest a previously unrecognised gonad phenotype caused

by disruption of the primary cilium, and raise the possibility of gonadal defects in Jeune and Sensenbrenner syndrome patients.

The role of the primary cilium in gonadal cells

In general, the presence of a primary cilium is associated with cells not undergoing mitosis since the anchor of the cilium is the basal body, a structure that derives from the mother centriole (Fonte et al., 1971; Seeley and Nachury, 2010). However, there is discordance in the role of cell cycle and ciliogenesis observed between *in vitro* and *in vivo* systems. In cell culture, most cells ciliate only after exit from the cell cycle, whereas, *in vivo,* a myriad of rapidly mitosing cells have a primary cilium (Fonte et al., 1971; Goetz et al., 2012; Ocbina et al., 2011). Furthermore, some differentiated cell types also lack a primary cilium, *in vivo* (Aughsteen, 2001). Our observations defining which gonadal cell types have a primary cilium did not necessarily correlate with what is known about the cell cycle in those lineages. Testicular germ cells at 12.5 dpc stop proliferating and enter G0/G1 arrest, whereas ovarian germ cells continue to proliferate and undergo meiosis at 13.5 dpc (Bowles et al., 2006; Hilscher, 1974). Thus, it was surprising that a primary cilium was not detected in testicular germ cells at 13.5 dpc but in some ovarian germ cells. On the other hand, foetal Leydig cells have no detectable mitotic activity once they have differentiated (Orth, 1982) and we found that the majority of Leydig cells have a primary cilium. Our observations confirm a previous report of primary cilia in Leydig cells, peritubular and other fibroblast-like stromal cells in the adult human testis (Takayama, 1981).

In the developing ovary, a lack of molecular markers has thus far hindered examination of the origin and specification of different somatic cell lineages. In a previous *in situ* hybridisation screen, novel domains of somatic cell gene expression were described suggesting that molecular regionalisation occurs earlier than previously thought (Chen et al., 2012). Consistent with these observations, we observed regionalisation of the prevalence of primary cilia on somatic cells. This suggests that subsets of ovarian somatic cells respond differently to intercellular signalling pathways and are more susceptible to some signalling perturbations. For example, activation of the Hh pathway in the foetal ovary leads to ectopic differentiation of Leydig cells, without further masculinisation of the gonad (Barsoum et al., 2009). Since Hh signalling is transduced via the primary cilium, perhaps trans-differentiated steroidogenic cells in hedgehog gain-of-function ovaries are the more commonly ciliated cells that we observed at the gonad-mesonephric boundary or towards the coelomic epithelium.

Testis cord morphogenesis in Ift144^{twt} mice

Testis cords are required for maturation of XY germ cells to spermatozoa, to create an immune privileged environment, to protect germ cells from exogenous signals and export spermatozoa to the male reproductive tract. The prevailing view of testis cord morphogenesis supports a model in which: (1) Sertoli cells cluster around groups of germ cells; (2) endothelial cells migrate in streams from the mesonephros to direct the partitioning of the XY gonad into cord domains; and (3) the XY gonad is patterned into definitive cords by peritubular myoid cells surrounding the cords and deposition of a basement membrane (Combes et al., 2009b; Cool et al., 2008; Coveney et al., 2008; Svingen and Koopman, 2013). It is thought that testis cords formation is triggered stochastically, since there is some variation in the number and size of the initial "pre-cord" domains (Combes et al., 2009a). However, the regularity of the shape and size of mature looped cord structures suggests that some yet unknown genetic control may regulate the patterning of testis cords. It was previously unclear if the XY gonad domain was partitioned a relatively stereotypical number of times or whether it is partitioned along the available space. Our data demonstrates the latter, suggesting that as long as XY gonad tissue is present and correctly patterned, endothelial cells will be induced along the length of the gonad domain. These findings help to further define testis cord morphogenesis, supporting a model in which the number of testis cords is determined by the size of the gonad domain.

Early extension of the gonad domain in Ift144^{twt} mice

The correct molecular sex patterning extended along the length of the genital ridge and germ cells were localised to the gonad poles of the in *Ift144^{twt}* embryos. In the XY genital ridge, the male sex-determining gene *Sry* is expressed in a dynamic wave, first in the centre of the gonad and subsequently expanding to the gonad anterior and posterior poles (Bullejos and Koopman, 2001). Moreover, FGF9 acts as a diffusible factor to drive centre-to-pole XY tubulogenic development (Hiramatsu et al., 2010). Delay in the expansion of the centre-to-pole wave of XY gene expression can result in the formation of ovotestes (Bullejos and Koopman, 2005; Wilhelm et al., 2009). Despite the genital ridge in *Ift144^{twt}* mice being approximately 1.4 times the length of wild-type, male sex determination and testis cord morphogenesis occurred along the entire length of the gonad axis, with no evidence of sex reversal at the poles. This implies that regardless of the distance, a level of robustness in the regulation of *Sry* expression exists, since the wave of male sex determination gene expression was completed within the critical temporal and spatial window.

It was clear that the gonads were expanded anteriorly in *Ift144^{twt}* embryos, relative to other organs such as the kidney and bladder. However, it is likely that it is the middle and/or posterior regions of the gonad that expand to cause the increased length rather than an expansion of the gonad anterior pole or a generalised anterior expansion, since the length of the mesonephric tubule domain was unchanged.

Interestingly, expansion of the gonad domain anteriorly in *Ift144^{twt}* embryos resulted in mis-localised ovaries in XX embryos to a more anterior position on the ventral side of the kidney, but correctly positioned testes in XY embryos. This may be a consequence of the normal sex-specific differences in the gubernaculum, a small muscular ligament attached to the gonads. In XY embryos, the gubernaculum anchors the testes to the inguinal region as the kidneys and the abdominal cavity expand anteriorly, whereas in XX embryos, the gubernaculum elongates with the expansion of the body cavity resulting in the ascent of the ovaries relative to the inguinal region (Shono et al., 1994). Since the anterior limit of both *Ift144^{twt}* testes and ovaries relative to the kidney is more cranial compared to wild-type, it is likely that the gubernaculum anchors *Ift144^{twt}* testes to maintain a normal position in the body cavity whereas *Ift144^{twt}* ovaries are more "free-floating", resulting in the ovaries maintaining a more anterior position on the ventral surface of the kidneys.

One of the key questions arising from analysis of *Ift144^{twt}* embryos is whether the expanded gonadal domain is a consequence of a gonad-intrinsic or extrinsic primary cilia-mediated signalling defect. Our finding of a concomitant expansion of the embryonic trunk domain in *Ift144^{twt}* embryos supports the latter. There are several lines of evidence demonstrating the importance of correct embryonic trunk extension on the extension of the coelomic epithelium and intermediate mesoderm. First, *Wnt5a*-null gonads display a reduced anterior–posterior axis, concurrent with a reduction in the extension of the trunk and tail of the embryo (Chawengsaksophak et al., 2012; Yamaguchi et al., 1999), supporting a link between trunk axis extension and gonad domain length. Second, live-imaging in chick embryos has observed that the Wolffian duct migrates in register with somite segmentation (Atsuta et al., 2013), suggesting that somite segmentation and Wolffian duct extension are a coupled process. Third, in the absence of the paraxial mesoderm in *Foxc1*; *Foxc2* double-null

embryos, the intermediate mesoderm is disorganised and fails to extend posteriorly (Wilm et al., 2004). Finally, the metanephric mesenchyme may be derived from more nascent posterior mesoderm cell progenitors in the tail bud, rather than the more anterior intermediate mesoderm, supporting a role for anterior–posterior extension in determining mesonephric/metanephric specification (Taguchi et al., 2014). Therefore, it is most likely that extension of the embryonic trunk is the cause of increased gonadal domain length in *Ift144*^{twt} embryos, although, we cannot completely exclude a contribution of gonad-intrinsic primary cilium-mediated signalling to the phenotype.

Related to this issue is the question of what these extrinsic signals might be. Factors driving extrinsic urogenital patterning are likely to include *Hox* paralog expression, WNT and retinoic acid signalling, all of which are required for posterior development of the embryo (Abu-Abed et al., 2001; Dunty et al., 2008; Wellik et al., 2002; Yun et al., 2014). It was recently reported that recapitulating the signalling dynamics in the posterior of the embryo by phasic WNT and retinoic acid signalling allows pluripotent cells to be differentiated to metanephric progenitors *in vitro* (Taguchi et al., 2014), demonstrating the importance of these signals to urogenital induction. While the aforementioned factors are likely to be important in the determination of mesonephric/metanephric patterning, it is still unclear whether specific signalling pathways in the embryonic trunk regulate gonad domain size or if it is merely the position of pro-metanephric/anti-mesonephric signals within the hind limb region that specifies the posterior limit of the gonad.

Implications for human ciliopathies

The present study represents the first detailed analysis of the embryonic gonadal phenotype of a mouse mutant with primary cilia trafficking defects. Like a number of IFT-A mouse mutants, *Ift144*^{twt} mice display a complex phenotype involving an expansion of ligand-independent hedgehog signalling in some contexts, while cells derived from these embryos show a reduced ability to respond to upstream activation of the pathway (Ashe et al., 2012; Liem et al., 2012). Notably, other IFT-A mouse mutants show a similar rib branching phenotype including *Ift140*^{cauli} and *Ift139*^{alien} (Herron et al., 2002; Miller et al., 2013), suggesting that they may also have an expanded gonad domain. Having shown that primary cilia are present in the embryonic gonad, it would be interesting to examine other mouse mutants with perturbed primary cilia trafficking such as IFT-B mutants, which predominantly show reduced Hedgehog signalling, for example *Ift88* hypomorphic mice (Liu et al., 2005). However, to our knowledge, no reported IFT-B mouse mutants have a similar somite/rib phenotype to *Ift144*^{twt} embryos, suggesting that the gonad domain would not be expanded in these mice.

Our finding that *Ift144*^{twt} embryonic gonads are larger than wild-type is inconsistent with gonadal hypoplasia identified in some human ciliopathies (Green et al., 1989; Klein and Ammann, 1969; McLoughlin and Shanklin, 1967). However, it is possible that these cases of reported hypogonadism are secondary to hypothalamic defects (Perez-Palacios et al., 1977; Soliman et al., 1996; Toledo et al., 1977), whereas gonad hyperplasia in *Ift144*^{twt} embryos clearly results from primary defects in embryo patterning. Analysis of additional primary cilia biogenesis and trafficking mouse mutants will help to further define the function of primary cilia signalling in embryonic gonad patterning and differentiation, and clarify reproductive phenotypes of individuals with ciliopathies.

Acknowledgements

We thank Tara-Lynne Davidson for assistance with mouse breeding. We thank Andrew Courtney for providing the samples shown in Fig. 7. This work was supported by research grants from the Australian Research Council and National Health and Medical Research Council (NHMRC) of Australia. Confocal microscopy was performed at the Australian Cancer Research Foundation Dynamic Imaging Centre for Cancer Biology. PK is a Senior Principal Research Fellow of the NHMRC. CW is a UQ Vice-Chancellor's Senior Research Fellow.

Appendix A. Supporting information

Supplementary data associated with this article can be found in the online version at http://dx.doi.org/10.1016/j.ydbio.2014.08.037.

References

Abu-Abed, S., Dolle, P., Metzger, D., Beckett, B., Chambon, P., Petkovich, M., 2001. The retinoic acid-metabolizing enzyme, CYP26A1, is essential for normal hindbrain patterning, vertebral identity, and development of posterior structures. Genes Dev. 15, 226–240.

Ashe, A., Butterfield, N.C., Town, L., Courtney, A.D., Cooper, A.N., Ferguson, C., Barry, R., Olsson, F., Liem Jr., K.F., Parton, R.G., Wainwright, B.J., Anderson, K.V., Whitelaw, E., Wicking, C., 2012. Mutations in mouse Ift144 model the craniofacial, limb and rib defects in skeletal ciliopathies. Hum. Mol. Genet. 21, 1808–1823.

Atsuta, Y., Tadokoro, R., Saito, D., Takahashi, Y., 2013. Transgenesis of the Wolffian duct visualizes dynamic behavior of cells undergoing tubulogenesis *in vivo*. Dev. Growth Differ. 55, 579–590.

Aughsteen, A.A., 2001. The ultrastructure of primary cilia in the endocrine and excretory duct cells of the pancreas of mice and rats. Eur. J. Morphol. 39, 277–283.

Barsoum, I.B., Bingham, N.C., Parker, K.L., Jorgensen, J.S., Yao, H.H., 2009. Activation of the Hedgehog pathway in the mouse fetal ovary leads to ectopic appearance of fetal Leydig cells and female pseudohermaphroditism. Dev. Biol. 329, 96–103.

Bouchard, M., Souabni, A., Mandler, M., Neubuser, A., Busslinger, M., 2002. Nephric lineage specification by Pax2 and Pax8. Genes Dev. 16, 2958–2970.

Bowles, J., Knight, D., Smith, C., Wilhelm, D., Richman, J., Mamiya, S., Yashiro, K., Chawengsaksophak, K., Wilson, M.J., Rossant, J., Hamada, H., Koopman, P., 2006. Retinoid signaling determines germ cell fate in mice. Science 312, 596–600.

Bredrup, C., Saunier, S., Oud, M.M., Fiskerstrand, T., Hoischen, A., Brackman, D., Leh, S. M., Midtbo, M., Filhol, E., Bole-Feysot, C., Nitschke, P., Gilissen, C., Haugen, O.H., Sanders, J.S., Stolte-Dijkstra, I., Mans, D.A., Steenbergen, E.J., Hamel, B.C., Matignon, M., Pfundt, R., Jeanpierre, C., Boman, H., Rodahl, E., Veltman, J.A., Knappskog, P.M., Knoers, N.V., Roepman, R., Arts, H.H., 2011. Ciliopathies with skeletal anomalies and renal insufficiency due to mutations in the IFT-A gene WDR19. Am. J. Hum. Genet. 89, 634–643.

Bullejos, M., Koopman, P., 2001. Spatially dynamic expression of Sry in mouse genital ridges. Dev. Dyn. 221, 201–205.

Bullejos, M., Koopman, P., 2005. Delayed Sry and Sox9 expression in developing mouse gonads underlies B6-Y(DOM) sex reversal. Dev. Biol. 278, 473–481.

Chawengsaksophak, K., Svingen, T., Ng, E.T., Epp, T., Spiller, C.M., Clark, C., Cooper, H., Koopman, P., 2012. Loss of Wnt5a disrupts primordial germ cell migration and male sexual development in mice. Biol. Reprod. 86, 1–12.

Chen, H., Palmer, J.S., Thiagarajan, R.D., Dinger, M.E., Lesieur, E., Chiu, H., Schulz, A., Spiller, C., Grimmond, S.M., Little, M.H., Koopman, P., Wilhelm, D., 2012. Identification of novel markers of mouse fetal ovary development. PLoS One 7, e41683.

Combes, A.N., Lesieur, E., Harley, V.R., Sinclair, A.H., Little, M.H., Wilhelm, D., Koopman, P., 2009a. Three-dimensional visualization of testis cord morphogenesis, a novel tubulogenic mechanism in development. Dev. Dyn. 238, 1033–1041.

Combes, A.N., Wilhelm, D., Davidson, T., Dejana, E., Harley, V., Sinclair, A., Koopman, P., 2009b. Endothelial cell migration directs testis cord formation. Dev. Biol. 326, 112–120.

Cool, J., Carmona, F.D., Szucsik, J.C., Capel, B., 2008. Peritubular myoid cells are not the migrating population required for testis cord formation in the XY gonad. Sex Dev. 2, 128–133.

Corbit, K.C., Aanstad, P., Singla, V., Norman, A.R., Stainier, D.Y., Reiter, J.F., 2005. Vertebrate smoothened functions at the primary cilium. Nature 437, 1018–1021.

Coveney, D., Cool, J., Oliver, T., Capel, B., 2008. Four-dimensional analysis of vascularization during primary development of an organ, the gonad. Proc. Natl. Acad. Sci. U. S. A. 105, 7212–7217.

Duldulao, N.A., Lee, S., Sun, Z., 2009. Cilia localization is essential for *in vivo* functions of the Joubert syndrome protein Arl13b/Scorpion. Development 136, 4033–4042.

Dunty Jr., W.C., Biris, K.K., Chalamalasetty, R.B., Taketo, M.M., Lewandoski, M., Yamaguchi, T.P., 2008. Wnt3a/beta-catenin signaling controls posterior body development by coordinating mesoderm formation and segmentation. Development 135, 85–94.

Ezratty, E.J., Stokes, N., Chai, S., Shah, A.S., Williams, S.E., Fuchs, E., 2011. A role for the primary cilium in Notch signaling and epidermal differentiation during skin development. Cell 145, 1129–1141.

Fehrenbach, H., Decker, C., Eisenberger, T., Frank, V., Hampel, T., Walden, U., Amann, K.U., Kruger-Stollfuss, I., Bolz, H.J., Haffner, K., Pohl, M., Bergmann, C., 2014. Mutations in WDR19 encoding the intraflagellar transport component IFT144 cause a broad spectrum of ciliopathies. Pediatr. Nephrol.
Fonte, V.G., Searls, R.L., Hilfer, S.R., 1971. The relationship of cilia with cell division and differentiation. J. Cell Biol. 49, 226–229.
Ginsburg, M., Snow, M.H., McLaren, A., 1990. Primordial germ cells in the mouse embryo during gastrulation. Development 110, 521–528.
Goetz, S.C., Anderson, K.V., 2010. The primary cilium: a signalling centre during vertebrate development. Nat. Rev. Genet. 11, 331–344.
Goetz, S.C., Liem Jr., K.F., Anderson, K.V., 2012. The spinocerebellar ataxia-associated gene Tau tubulin kinase 2 controls the initiation of ciliogenesis. Cell 151, 847–858.
Green, J.S., Parfrey, P.S., Harnett, J.D., Farid, N.R., Cramer, B.C., Johnson, G., Heath, O., McManamon, P.J., O'Leary, E., Pryse-Phillips, W., 1989. The cardinal manifestations of Bardet–Biedl syndrome, a form of Laurence–Moon–Biedl syndrome. N. Engl. J. Med. 321, 1002–1009.
Grote, D., Souabni, A., Busslinger, M., Bouchard, M., 2006. Pax 2/8-regulated Gata 3 expression is necessary for morphogenesis and guidance of the nephric duct in the developing kidney. Development 133, 53–61.
Habbig, S., Bartram, M.P., Sagmuller, J.G., Griessmann, A., Franke, M., Muller, R.U., Schwarz, R., Hoehne, M., Bergmann, C., Tessmer, C., Reinhardt, H.C., Burst, V., Benzing, T., Schermer, B., 2012. The ciliopathy disease protein NPHP9 promotes nuclear delivery and activation of the oncogenic transcriptional regulator TAZ. Hum. Mol. Genet. 21, 5528–5538.
Harikae, K., Miura, K., Kanai, Y., 2013. Early gonadogenesis in mammals: significance of long and narrow gonadal structure. Dev. Dyn. 242, 330–338.
Herron, B.J., Lu, W., Rao, C., Liu, S., Peters, H., Bronson, R.T., Justice, M.J., McDonald, J.D., Beier, D.R., 2002. Efficient generation and mapping of recessive developmental mutations using ENU mutagenesis. Nat. Genet. 30, 185–189.
Hilscher, W., 1974. Kinetics of prespermatogenesis and spermatogenesis. Verh. Anat. Ges. 68, 39–62.
Hiramatsu, R., Harikae, K., Tsunekawa, N., Kurohmaru, M., Matsuo, I., Kanai, Y., 2010. FGF signaling directs a center-to-pole expansion of tubulogenesis in mouse testis differentiation. Development 137, 303–312.
Karl, J., Capel, B., 1998. Sertoli cells of the mouse testis originate from the coelomic epithelium. Dev. Biol. 203, 323–333.
Klein, D., Ammann, F., 1969. The syndrome of Laurence–Moon–Bardet–Biedl and allied diseases in Switzerland. Clinical, genetic and epidemiological studies. J. Neurol. Sci. 9, 479–513.
Kume, T., Deng, K., Hogan, B.L., 2000. Murine forkhead/winged helix genes Foxc1 (Mf1) and Foxc2 (Mfh1) are required for the early organogenesis of the kidney and urinary tract. Development 127, 1387–1395.
Lawson, K.A., Hage, W.J., 1994. Clonal analysis of the origin of primordial germ cells in the mouse. Ciba. Found. Symp. 182, 68–84 (discussion 84-91).
Liem Jr., K.F., Ashe, A., He, M., Satir, P., Moran, J., Beier, D., Wicking, C., Anderson, K.V., 2012. The IFT-A complex regulates Shh signaling through cilia structure and membrane protein trafficking. J. Cell Biol. 197, 789–800.
Liu, A., Wang, B., Niswander, L.A., 2005. Mouse intraflagellar transport proteins regulate both the activator and repressor functions of Gli transcription factors. Development 132, 3103–3111.
Mattiske, D., Kume, T., Hogan, B.L., 2006. The mouse forkhead gene Foxc1 is required for primordial germ cell migration and antral follicle development. Dev. Biol. 290, 447–458.
McFarlane, L., Truong, V., Palmer, J.S., Wilhelm, D., 2013. Novel PCR assay for determining the genetic sex of mice. Sex. Dev. 7, 207–211.
McLaren, A., Lawson, K.A., 2005. How is the mouse germ-cell lineage established? Differentiation 73, 435–437.
McLoughlin, T.G., Shanklin, D.R., 1967. Pathology of Laurence–Moon–Bardet–Biedl syndrome. J. Pathol. Bacteriol. 93, 65–79.
Miller, K.A., Ah-Cann, C.J., Welfare, M.F., Tan, T.Y., Pope, K., Caruana, G., Freckmann, M.L., Savarirayan, R., Bertram, J.F., Dobbie, M.S., Bateman, J.F., Farlie, P.G., 2013. Cauli: a mouse strain with an Ift140 mutation that results in a skeletal ciliopathy modelling Jeune syndrome. PLoS Genet. 9, e1003746.
Neugebauer, J.M., Amack, J.D., Peterson, A.G., Bisgrove, B.W., Yost, H.J., 2009. FGF signalling during embryo development regulates cilia length in diverse epithelia. Nature 458, 651–654.
Ocbina, P.J., Eggenschwiler, J.T., Moskowitz, I., Anderson, K.V., 2011. Complex interactions between genes controlling trafficking in primary cilia. Nat. Genet. 43, 547–553.
Ohinata, Y., Payer, B., O'Carroll, D., Ancelin, K., Ono, Y., Sano, M., Barton, S.C., Obukhanych, T., Nussenzweig, M., Tarakhovsky, A., Saitou, M., Surani, M.A., 2005. Blimp1 is a critical determinant of the germ cell lineage in mice. Nature 436, 207–213.
Orth, J.M., 1982. Proliferation of Sertoli cells in fetal and postnatal rats: a quantitative autoradiographic study. Anat. Rec. 203, 485–492.
Ou, G., Blacque, O.E., Snow, J.J., Leroux, M.R., Scholey, J.M., 2005. Functional coordination of intraflagellar transport motors. Nature 436, 583–587.
Pazour, G.J., Dickert, B.L., Vucica, Y., Seeley, E.S., Rosenbaum, J.L., Witman, G.B., Cole, D.G., 2000. Chlamydomonas IFT88 and its mouse homologue, polycystic kidney disease gene tg737, are required for assembly of cilia and flagella. J. Cell Biol. 151, 709–718.
Perez-Palacios, G., Uribe, M., Scaglia, H., Lisker, R., Pasapera, A., Maillard, M., Medina, M., 1977. Pituitary and gonadal function in patients with the Laurence–Moon–Biedl syndrome. Acta Endocrinol. (Cph.) 84, 191–199.
Saxen, L., Sariola, H., 1987. Early organogenesis of the kidney. Pediatr. Nephrol. 1, 385–392.
Schneider, L., Clement, C.A., Teilmann, S.C., Pazour, G.J., Hoffmann, E.K., Satir, P., Christensen, S.T., 2005. PDGFRalphaalpha signaling is regulated through the primary cilium in fibroblasts. Curr. Biol. 15, 1861–1866.
Seeley, E.S., Nachury, M.V., 2010. The perennial organelle: assembly and disassembly of the primary cilium. J. Cell Sci. 123, 511–518.
Shono, T., Ramm-Anderson, S., Hutson, J.M., 1994. Transabdominal testicular descent is really ovarian ascent. J. Urol. 152, 781–784.
Soliman, A.T., Rajab, A., AlSalmi, I., Asfour, M.G., 1996. Empty sellae, impaired testosterone secretion, and defective hypothalamic-pituitary growth and gonadal axes in children with Bardet–Biedl syndrome. Metabolism 45, 1230–1234.
Svingen, T., Koopman, P., 2013. Building the mammalian testis: origins, differentiation, and assembly of the component cell populations. Genes Dev. 27, 2409–2426.
Svingen, T., Spiller, C.M., Kashimada, K., Harley, V.R., Koopman, P., 2009. Identification of suitable normalizing genes for quantitative real-time RT-PCR analysis of gene expression in fetal mouse gonads. Sex. Dev. 3, 194–204.
Szabo, P.E., Hubner, K., Scholer, H., Mann, J.R., 2002. Allele-specific expression of imprinted genes in mouse migratory primordial germ cells. Mech. Dev. 115, 157–160.
Taguchi, A., Kaku, Y., Ohmori, T., Sharmin, S., Ogawa, M., Sasaki, H., Nishinakamura, R., 2014. Redefining the *in vivo* origin of metanephric nephron progenitors enables generation of complex kidney structures from pluripotent stem cells. Cell Stem Cell 14, 53–67.
Takayama, H., 1981. Single cilia formation in cells of the testicular interstitium in fertile men. Int. J. Androl. 4, 246–256.
Toledo, S.P., Medeiros-Neto, G.A., Knobel, M., Mattar, E., 1977. Evaluation of the hypothalamic-pituitary-gonadal function in the Bardet–Biedl syndrome. Metabolism 26, 1277–1291.
Warr, N., Bogani, D., Siggers, P., Brixey, R., Tateossian, H., Dopplapudi, A., Wells, S., Cheeseman, M., Xia, Y., Ostrer, H., Greenfield, A., 2011. Minor abnormalities of testis development in mice lacking the gene encoding the MAPK signalling component, MAP3K1. PLoS One 6, e19572.
Wellik, D.M., Hawkes, P.J., Capecchi, M.R., 2002. Hox11 paralogous genes are essential for metanephric kidney induction. Genes Dev. 16, 1423–1432.
Wilhelm, D., Washburn, L.L., Truong, V., Fellous, M., Eicher, E.M., Koopman, P., 2009. Antagonism of the testis- and ovary-determining pathways during ovotestis development in mice. Mech. Dev. 126, 324–336.
Wilm, B., James, R.G., Schultheiss, T.M., Hogan, B.L., 2004. The forkhead genes, Foxc1 and Foxc2, regulate paraxial *versus* intermediate mesoderm cell fate. Dev. Biol. 271, 176–189.
Yamaguchi, T.P., Bradley, A., McMahon, A.P., Jones, S., 1999. A Wnt5a pathway underlies outgrowth of multiple structures in the vertebrate embryo. Development 126, 1211–1223.
Yao, H.H., Whoriskey, W., Capel, B., 2002. Desert Hedgehog/Patched 1 signaling specifies fetal Leydig cell fate in testis organogenesis. Genes Dev. 16, 1433–1440.
Yun, K., Ajima, R., Sharma, N., Costantini, F., Mackem, S., Lewandoski, M., Yamaguchi, T.P., Perantoni, A.O., 2014. Non-canonical Wnt5a/Ror2 signaling regulates kidney morphogenesis by controlling intermediate mesoderm extension. Hum. Mol. Genet (ahead of print).